catalysts

MDPI

Article

Converting Hybrid Mechanisms to Electron Transfer Mechanism by Increasing Biochar Pyrolysis Temperature for the Degradation of Sulfamethoxazole in a Sludge Biochar/Periodate System

Liuyang He [1], Shangding Yang [1], Lie Yang [1,*], Yulong Li [1], Dejin Kong [1], Li Wu [1] and Zulin Zhang [1,2,*]

[1] Hubei Key Laboratory of Mineral Resources Processing and Environment, School of Resources and Environmental Engineering, Wuhan University of Technology, Wuhan 430070, China
[2] The James Hutton Institute, Craigiebuckler, Aberdeen ABI5 8QH, UK
* Correspondence: yanglie612@whut.edu.cn (L.Y.); zulin.zhang@hutton.ac.uk (Z.Z.)

Abstract: In this study, sludge biochar was prepared under four pyrolysis temperatures (SBC300, SBC500, SBC700, and SBC900) and then was employed to activate periodate (PI) for the degradation of sulfamethoxazole (SMX). Various characterization methods were employed to investigate the effect of pyrolysis temperature on the physicochemical properties of sludge biochar and the activation capacity of periodate. The SMX adsorption capacity of SBCs and the ability of activating PI to degrade SMX increased with the increasing pyrolysis temperature. The degradation of SMX by the SBCs/PI systems was highly dependent on the initial pH of the solution and the dosage of SBCs. Mechanistic studies indicated that the degradation of SMX by the SBCs/PI system was mainly based on an electron-mediated transfer mechanism. Additionally, the electron transfer capacity of the SBCs affected the defects and the degree of graphitization. The contribution of free radicals to SMX degradation decreases with increasing pyrolysis temperature. Toxicity experiments demonstrated that the toxic elimination of SMX by the SBCs/PI system was enhanced with increasing pyrolysis temperature.

Keywords: pyrolysis temperature; sludge biochar; periodate; nonradical degradation; electron transfer

Citation: He, L.; Yang, S.; Yang, L.; Li, Y.; Kong, D.; Wu, L.; Zhang, Z. Converting Hybrid Mechanisms to Electron Transfer Mechanism by Increasing Biochar Pyrolysis Temperature for the Degradation of Sulfamethoxazole in a Sludge Biochar/Periodate System. *Catalysts* **2022**, *12*, 1431. https://doi.org/10.3390/catal12111431

Academic Editor: María Victoria Navarro

Received: 6 October 2022
Accepted: 4 November 2022
Published: 14 November 2022

1. Introduction

With the rapid urbanization and industrialization in developing countries in recent decades, the number of urban wastewater treatment plants for purifying urban domestic wastewater has been growing rapidly along with urbanization [1,2]. Urban sewage sludge is an unavoidable by-product of the sewage treatment process in urban wastewater treatment plants, and the sludge production in China exceeds 20 million tons per year [3]. The treatment and disposal expenses exceed 31.2 billion RMB per year [4]. Sewage sludge generally contains large amounts of nitrogen, phosphorus compounds, organic pollutants (antibiotics, persistent organic pollutants, etc.), pathogens, and heavy metals [5], while traditional sludge treatment and disposal methods such as landfilling, incineration, and composting are costly and may cause secondary environmental pollution [6]. Therefore, economical and environment-friendly sludge treatment and utilization have become research hotspots in recent years [7]. The pyrolysis treatment of sewage sludge is a promising treatment method that not only destroys most pathogens such as bacteria and fungi but also recovers sludge's calorific value to produce large amounts of biochar material [8].

Sludge biochar is the main product of the sewage sludge pyrolysis process, which is characterized by abundant surface nitrogen and oxygen functional groups, large specific surface area and excellent porous structure [9,10]. Because of its lower cost and excellent pore structure, sludge biochar is often used as an excellent carrier material for carbon-based catalysts [11]. Sludge biochar and its modified sludge-based biochar have

been widely used in adsorption and advanced oxidation processes (AOPs) to remove a wide range of inorganic and organic pollutants [12–14]. Periodate (PI)-based advanced oxidation processes have received extensive research and attention in recent years due to their ability to remove persistent organic pollutants economically and efficiently [15–17]. Due to the weak oxidation capacity of non-activated periodate for effectively oxidizing organic pollutants, environmentally friendly and efficient activation PI approaches have received greater research attention. Previous studies have shown that effective activation methods for PI include energy input (UV, ultrasound, etc.) [18], transition metals and metal oxides [19], carbon materials (carbon nanotubes, biochar, etc.) [15], alkaline conditions [20], and freezing [21]. The energy input activation method is energy-intensive and unsustainable, while transition metal-based catalysts are prone to environmental problems such as the leaching of heavy metals, and thus, biochar prepared by recycling waste resources has promising applications. Our previous studies have demonstrated that sludge-based biochar has the ability to activate periodate to degrade organic pollutants [22,23]. However, most previous studies have focused on the modified methods of sludge-based biochar for periodate activation, while the concern for the influences of biochar fabrication processes on the electron-mediated transfer activation of periodate and toxicity elimination of organic pollutants is lacking.

The yield and physicochemical properties of sludge biochar are greatly influenced by the raw material and pyrolysis parameters [24]. It has been demonstrated that the specific surface area, number and type of surface functional groups, heavy metal content, zero charge point (pH_{pzc}) and defect structure of sludge biochar are easily affected by the pyrolysis temperature [25,26]. The catalytic activation capacity of sludge biochar in AOPs depends mainly on physicochemical properties such as specific surface area, graphitization and defect structure, redox metal content, and oxygen-containing functional groups, which are all influenced by the pyrolysis temperature [27–29]. However, the properties of sludge biochar prepared at different pyrolysis temperatures have been little studied on the performance of activated periodate and the mechanism of degradation of pollutants.

Sulfamethoxazole (SMX) is one of the most widely used broad-spectrum antibiotics, and it is frequently detected in various water bodies because of its ineffective removal in conventional wastewater treatment plants [30,31]. Therefore, SMX was selected as the target pollutant in this study. Firstly, sludge biochar (SBCs) was prepared at four pyrolysis temperatures (300 °C, 500 °C, 700 °C, and 900 °C) at the same ramp-up rate. Secondly, the sludge biochar with different pyrolysis temperatures was characterized to investigate the effect of pyrolysis temperature on the physicochemical properties of sludge biochar and the active sites. Then, the performance of sludge biochar with different temperature pyrolysis for SMX adsorption and activated periodate degradation of SMX was investigated, and the effect of various reaction conditions such as pH, PI, and catalyst dosing on SMX degradation was also studied. Finally, the mechanism of SMX degradation by sludge biochar-activated periodate was determined by chemical quenching experiments, EPR, and characterization, and the acute toxicity of various systems was determined by plant germination experiments.

2. Results and Discussion

2.1. Characterizations of SBCs

The microscopic shape of four SBCs (SBC300, SBC500, SBC700, and SBC900) was recorded by SEM (Figures 1 and S1). Obvious irregular blocky structures were observed in the SEM images of SBCs. It was found that the change in pyrolysis temperature posed a remarkable effect on the surface morphological characteristics of SBCs. According to the SEM images of SBCs at different temperatures in Figure S1, it can be clearly observed that the surface pore structure of SBCs was more obvious and the size of the irregular block structure was smaller with the increase in pyrolysis temperature. Moreover, irregular pore structures were found more frequently on SBCs pyrolyzed at higher temperatures, indicating that higher pyrolysis temperatures may lead to an increase in the proportion of

amorphous carbon on the surface of SBCs. The EDS elemental mapping images (Figure 1) demonstrated that the surface of SBCs mainly contains C, O, Si, and N elements. Meanwhile, as shown in Table 1, the ratio of O/C on the surface of SBCs gradually increased with the increase in pyrolysis temperature. A higher O/C ratio would result in a better hydrophilicity and polarity of biochar [23]. In addition, the elemental N content on the surface of biochar gradually decreased at higher pyrolysis temperatures.

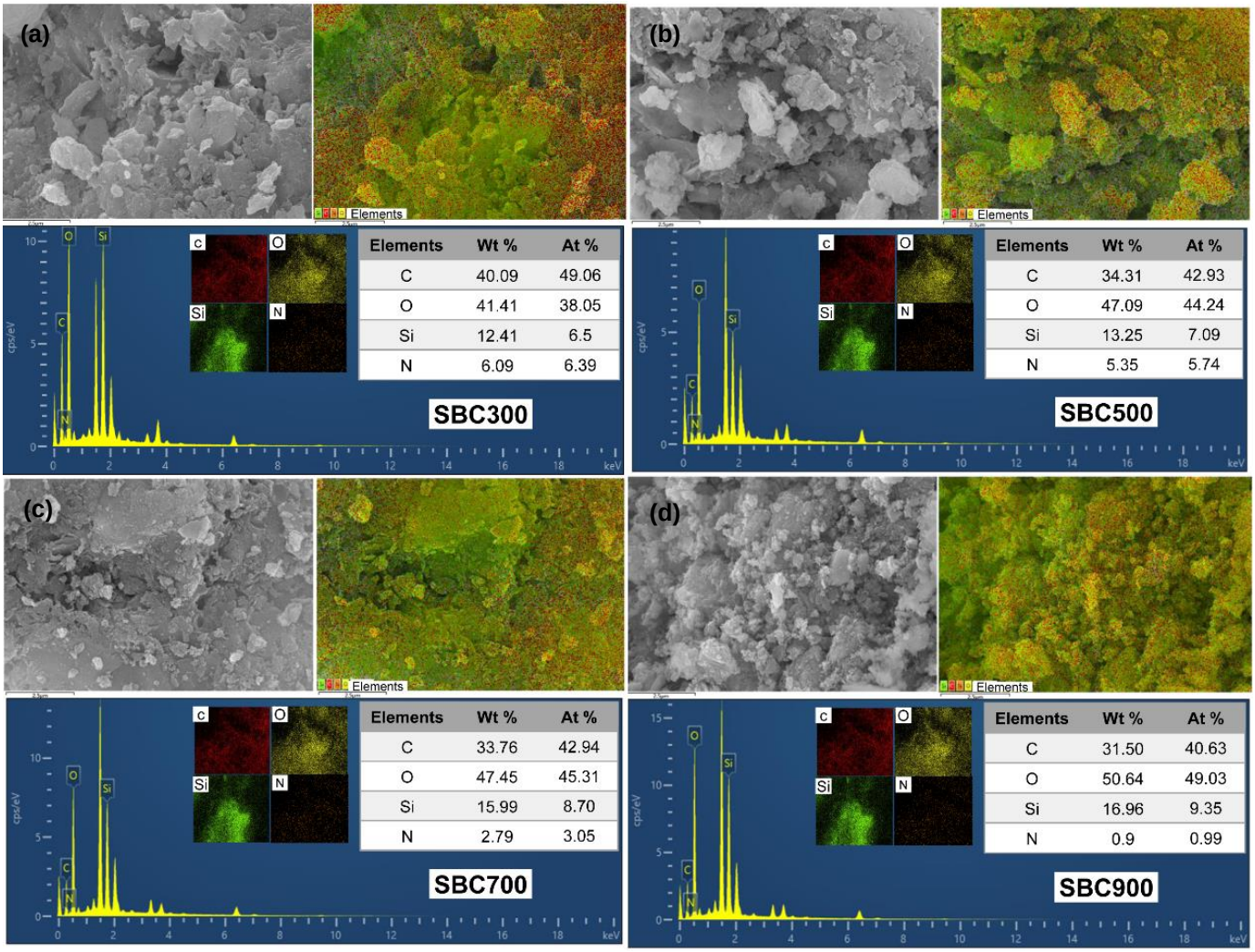

Figure 1. SEM-EDS images of SBCs: (**a**) SBC 300; (**b**) SBC 500; (**c**) SBC 700; (**d**) SBC 900.

Table 1. Textural properties of SBCs.

Catalysts	S_{BET} (m^2 g^{-1})	V_{tot} (cm^3 g^{-1})	D_p (nm)	O/C Ratio
SBC300	34.92	0.08942	10.64	1.03
SBC500	83.50	0.1200	8.93	1.37
SBC700	61.26	0.1798	12.34	1.41
SBC900	124.96	0.1934	6.791	1.61

Table 1 and Figure S2 showed the textural properties and N_2 adsorption–desorption isotherms of SBCs, respectively. The SBCs were all mesoporous materials and showed type IV adsorption isotherms. The abundant presence of micropores and mesopores in SBCs can be observed according to the pore size distribution plot in Figure S2. SBC300 possessed a minimum BET-specific surface area of 34.92 m^2 g^{-1}, and the BET specific surface

area came to 83.5 m^2 g^{-1} and 61.26 m^2 g^{-1} when the pyrolysis temperature was further increased to 500 °C and 700 °C, respectively. However, when the pyrolysis temperature was increased to 900 °C, SBC900 exhibited the maximum BET specific surface area up to 124.94 m^2 g^{-1}. This might be due to the blockage of pores in the biochar caused by the decomposition of elemental N in the sludge at 700 °C, which was also confirmed by the lower micropore density in the pore size distribution [32]. With the further increased pyrolysis temperature, the decomposition of elemental N was more complete, which also led to the unclogging influence of blocked pores. In addition, higher pyrolysis temperatures also lead to an increase in the proportion of graphitic N in the biochar, which enhances its activation capacity [33].

Figure 2a showed the XRD patterns of SBCs, indicating the existence of three peaks at 26.5°, 42.3°, and 59.9°, which can be attributed to (002), (100), and (103) planes of graphite carbon material (PDF#89-8487). The diffraction peaks at 20.8° (100), 36.5° (110), 39.4° (102), and 50.1° (112) could be assigned to SiO_2 (PDF#70-3755). The XRD results indicated that the pyrolysis temperature did not cause changes in the lattice structure of SBCs.

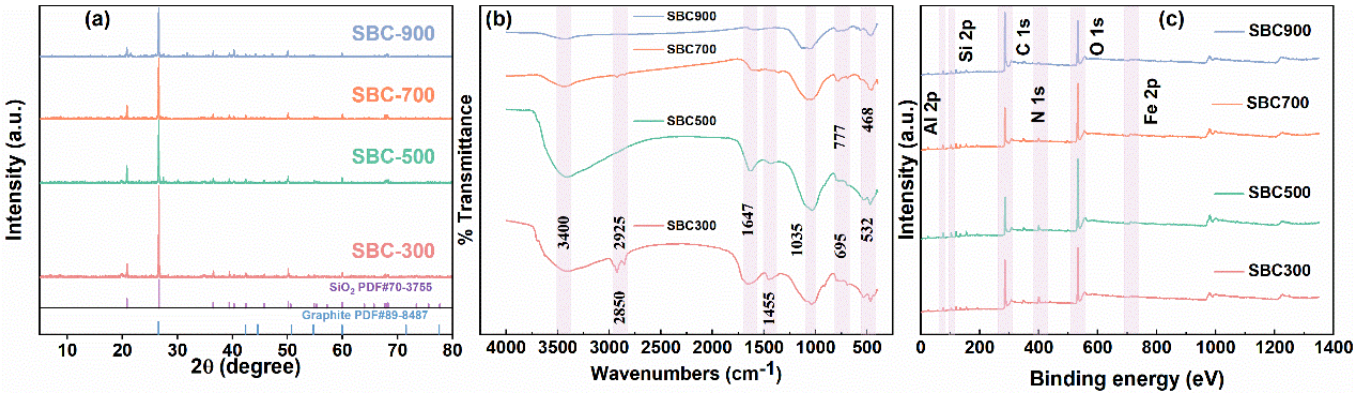

Figure 2. The (**a**) XRD spectra, (**b**) FTIR spectra, and (**c**) XPS spectra.

Figure 2b demonstrated the FTIR spectra of the SBCs which were employed to investigate the functional groups on the SBCs. It can be observed that the difference in the FTIR characteristic bands between SBCs was not significant. However, the band intensities of SBCs had a significant trend of weakening with the increase in pyrolysis temperature. Specifically, the wavelength at 2850 cm^{-1} and 2925 cm^{-1} of SBC300 were attributed to the stretching vibration of aliphatic -CH and -CH_2, which were not found in other SBCs. This may be attributed to the decomposition of organic aliphatic hydrocarbons at higher pyrolysis temperatures [34]. In addition, it can be observed that the intensity of the peak located around 3400 cm^{-1} (attributed to the hydroxyl group) decreased with the increase in the pyrolysis temperature, which may be attributed to the decrease in the oxygen-containing functional groups due to the increase in the pyrolysis temperature [35]. In the XPS survey spectra (Figure 2c), two main characteristic peaks at 285 eV and 533 eV were assigned to C1s and O1s. Meanwhile, the characteristic peak at 400 eV was corresponding to N1s, and its peak intensity decreased with increasing pyrolysis temperature, which was consistent with the EDS results. Meanwhile, the high-resolution XPS spectra of N1s is shown in Figure S3, and the characteristic peak of graphitic N was observed at the binding energies of 401.8 eV. Apparently, graphitic N appeared at SBC700, and its atomic ratio increased from 23% to 57% with the increase in pyrolysis temperature from 700 to 900 °C. The presence of graphitic N could facilitate the activation of the oxidant because it changes the charge density of the carbon network [36]. Figure S4 showed the high-resolution XPS spectra of C1s and O1s of SBCs. The fitted peaks could be assigned to C-C (284.8 eV), C-O (286.3 eV), O-C=O (288.6 eV), and C-O (532 eV). As the pyrolysis temperature increased, the characteristics of the C1s moieties changed significantly, in which the proportion of atoms in the C-C bond part increased significantly. Nonetheless, the proportion of atoms in the C-O bond

decreased gradually, which was consistent with the FTIR results. Meanwhile, the increase in the proportion of C-C bonds may also lead to the increase in defective structures in biochar.

Figure 3 demonstrated the Raman spectra of various SBCs to reveal the degree of defects in SBCs. The two obvious peaks located at 1350 cm^{-1} and 1580 cm^{-1} correspond to the D band and G band, respectively, where the D band indicated disordered carbon and the G band was associated with the sp^2 hybridized carbon network [37]. Meanwhile, the ratio of the intensity of the D and G bands (I_D/I_G) was used to reveal the degree of defects in the carbon material. Obviously, SBC900 showed the highest I_D/I_G value of 1.488, which was significantly higher compared to SBC300, SBC500, and SBC700 at 1.081, 1.241, and 1.348, indicating that higher pyrolysis temperatures significantly induced greater defective sites. Those defective sites could be used for the activation of PI and the adsorption of SMX. Particularly, the Raman spectra of SBC300 showed a broad peak with less pronounced D and G bands compared to other SBCs, indicating that the SBCs prepared at lower pyrolysis temperatures may not possess sufficient PI activation ability.

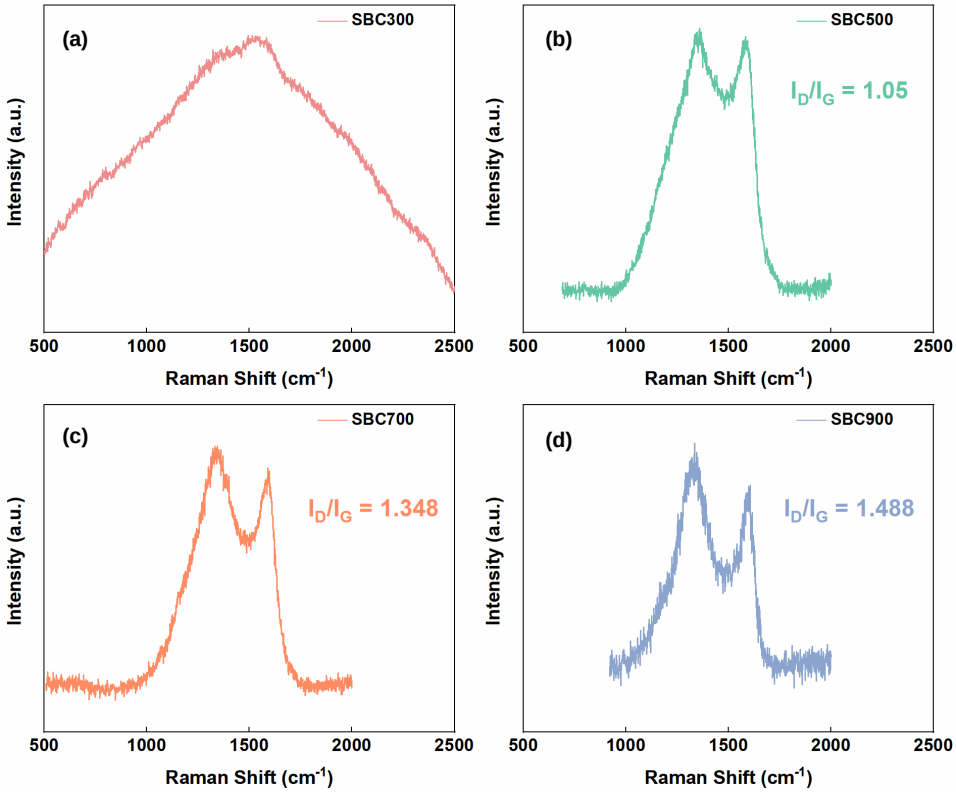

Figure 3. The Raman spectra of SBCs: (**a**) SBC 300; (**b**) SBC 500; (**c**) SBC 700; (**d**) SBC 900.

2.2. Activation Performance of SBCs towards PI for SMX Removal

The activation performance of SBCs towards PI was evaluated regarding the SMX as the target organic pollutant. Apparently, the removal of SMX by PI alone and adsorption of the SBC300 and SBC300/PI system were not significant, at 11.8%, 14.2%, and 19.9%, respectively (Figure 4). It was due to the fact that SBC300 did not have a large specific surface area and a defective structure, which were vital for the adsorption of SMX and the activation of PI [38]. The adsorption capacity of SBCs changed sharply with increasing pyrolysis temperature from 30.4% for SBC500 to 68.5% and 98.7% for SBC700 and SBC900. The BET specific surface area of SBC700 was smaller than that of SBC500, but its adsorption capacity was stronger than SBC500, indicating that the BET specific surface area was not the dominant factor in the adsorption of SBCs on SMX. The degree of defects and graphitization of SBCs increased with increasing pyrolysis temperature, and SBC900 possessed the highest degree of defects, indicating that the degree of defects may be the main factor for the

adsorption performance of SBCs on SMX. Obviously, SBC500, SBC700, and SBC900 showed strong PI activation ability when PI was introduced into the system, and the removal efficiency for SMX was significantly increased (Figure 4). The degradation efficiencies of SMX reached 79% (60 min), 99.7% (30 min) and 100% (5 min) for SBC500/PI, SBC700/PI and SBC900/PI, respectively. Meanwhile, the SMX degradation kinetics in the SBCs/PI system was investigated by employing pseudo-first-order models and shown in Table S1. It was observed that the R^2 of SBC500, SBC700 and SBC900 were 0.7798, 0.9921 and 0.7968, respectively, indicating that adsorption may have certain effects on the degradation process. The first-order rate k of the SBCs/PI system increased significantly with the increase in the pyrolysis temperature from 0.0219 min^{-1} for the SBC500/PI system to 0.1846 min^{-1} for the SBC700/PI system, and the k of the SBC900/PI system similarly increased to 0.3714 min^{-1}. Similarly, the superior PI activation ability exhibited by SBCs was also attributed to their defective sites that were enhanced with increasing pyrolysis temperature.

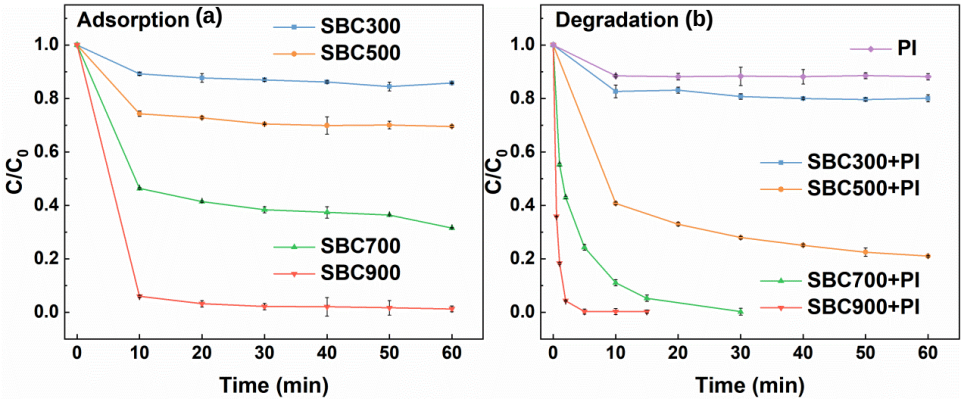

Figure 4. Removal performance of SMX by different systems: General conditions: [PI] = 1 mM, [catalyst] = 1.0 g L^{-1}, pH = 3.5, [SMX] = 5 mg L^{-1}.

Desorption experiments were performed to confirm that the adsorbed SMX in the system was degraded. The data in Table S2 showed that the adsorption capacities of SBC500, SBC700, and SBC900 at 60 min were 1.229 mg g^{-1}, 2.840 mg g^{-1}, and 4.809 mg g^{-1}, respectively, and their desorption rates were 47.1%, 33.1%, and 37.1%, respectively. The results indicated that 55.6%, 84.5%, and 96.2% of the adsorbed SMX were eventually degraded. Based on the above results, the capacity of SBC300 for SMX adsorption and activation of PI was extremely limited, and other SBCs would be focused on in subsequent experiments.

2.3. Influence of Reaction Conditions

Since SBCs/PI systems showed excellent SMX removal performance, the effect of pH was performed to further investigate the suitability of this system. Figure 5a–c presented the SMX degradation efficiency in the pH range 3–9 for the SBC500/PI, SBC700/PI, and SBC900/PI systems, respectively. Obviously, the SBC500/PI system and the SBC700/PI system were significantly affected by the initial pH, and the degradation rate of SMX decreased rapidly with increasing pH. The SBC500/PI system was most remarkably affected by the initial pH. When the initial pH was increased from 3 to 5, the degradation efficiency of SMX decreased from 86.3% to 38.0%, and then, the degradation efficiency of SMX gradually remained stable with the increase in the initial pH. Nevertheless, the SBC700/PI system was moderately influenced by the initial pH and the degradation efficiency of SMX decreased smoothly from 99.7% to 85.2% as the initial pH increased from 3 to 9. However, the degradation efficiency of SMX in the SBC900/PI system was only slightly affected by the initial pH of the solution. According to Figure S5, the zeta potential of both SBC500 and SBC700 maintained negative values in the pH range of 3 to 9, indicating that these SBCs maintain negative surface charges under a wide range of pH conditions. Meanwhile, the two pK_a values of SMX are 1.6 and 5.7 [39], suggesting that SMX will remain in the

molecular state or have a negative surface charge at pH greater than 1.6. Therefore, when the solution pH was greater than 5.7, the surfaces of SBC500, SBC700, and SMX were all negatively charged, and the increased electrostatic repulsion would continuously lead to a decrease in adsorption and catalytic activity [40]. Unsurprisingly, the value of zeta potential on the surface of SBC900 was kept in a small range, which caused the electrostatic repulsion to remain low as well, and this resulted in the SBC900/PI system remaining effective in degrading SMX over a wide pH range.

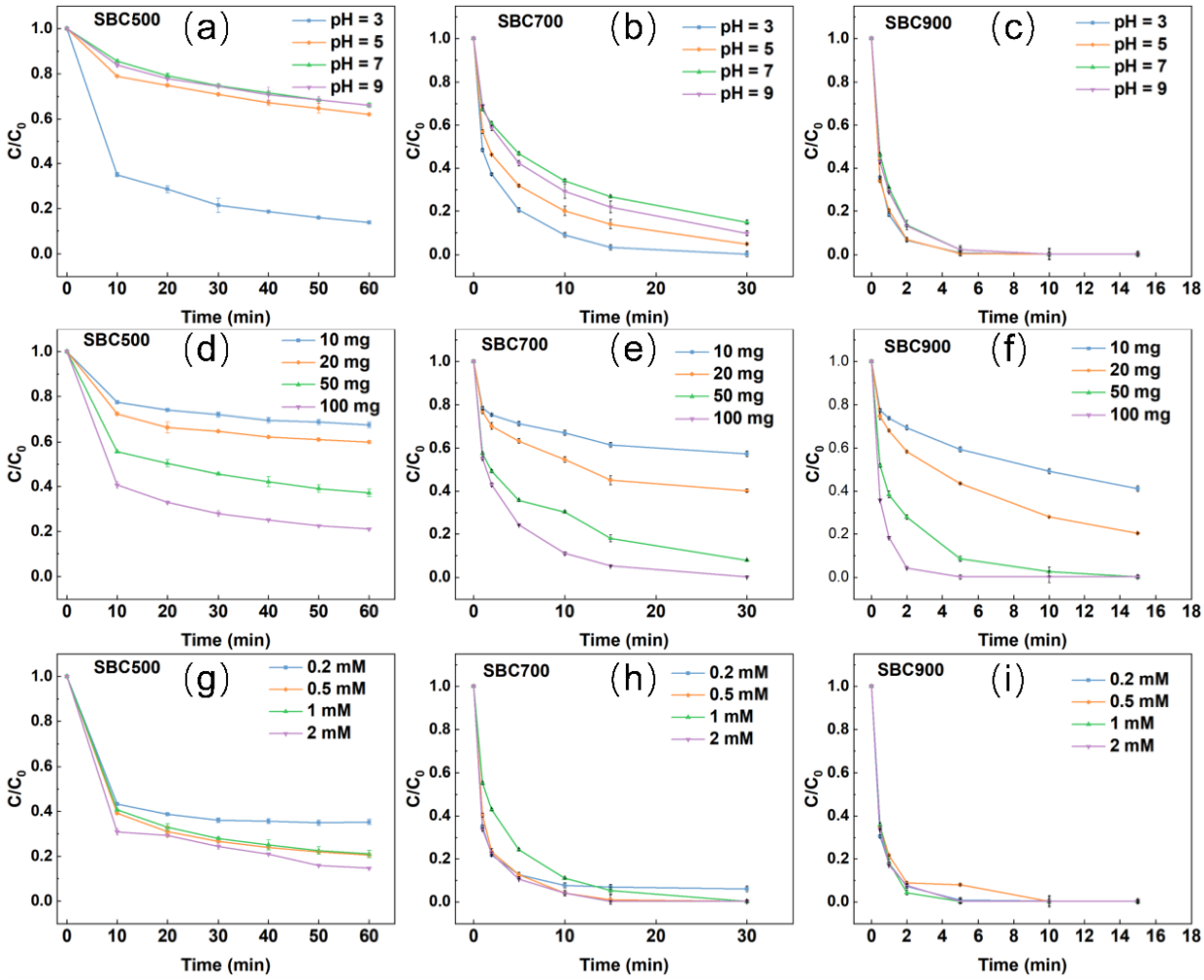

Figure 5. (**a**–**c**) The influence of initial pH on the degradation of SMX; (**d**–**f**) the influence of SBCs dosage on the degradation of SMX; (**g**–**i**) the influence of PI dosage on the degradation of SMX.

The effects of catalyst dosage and PI dosage on SMX degradation are presented in Figure 5. Obviously, at all SBCs/PI systems, increasing the catalyst dosage significantly enhanced the removal efficiencies of SMX. With the dosage of SBCs increased from 0.1 to 1 g L^{-1}, the degradation efficiency of SMX increased from 32.4% to 79.0% for the SBC500/PI system, from 42.6% to 99.7% for the SBC700/PI system, and from 58.9% to almost complete removal for the SBC900/PI system. Meanwhile, the degradation rates of SMX in all SBCs/PI systems increased significantly during the increasing dosage. Generally, larger catalyst dosages resulted in more PI activation sites, and further increasing catalyst dosage after achieving larger removal efficiencies did not show a decrease in efficiency, indicating that the number of catalyst active sites in the SBCs/PI system was the main factor controlling the reaction. Different from the catalyst dosage, the effect of increasing PI dosage on SMX degradation efficiency was not highly significant. Among all the SBCs/PI systems, the degradation efficiency and degradation rate of SMX reached the maximum

when the PI amount reached 0.5 mM, while the degradation of SMX basically remained at a high level when the PI amount was further increased. This result was consistent with previous studies [15]. This phenomenon indicated that the PI dosage of 0.5 mM was essentially saturated in the SBCs/PI system, and no inhibition was observed when the PI dosage further increased to 2 mM, which also revealed that the system degradation of SMX was highly dependent on the active site provided by the SBCs. Compared with other similar carbon catalyst dosages (granular-activated carbon = 1 g L^{-1}, iodine-doped granular activated carbon = 1 g L^{-1}) and PI dosages (granular-activated carbon = 10 mM, iodine-doped granular-activated carbon = 2.5 mM), this study possessed significant advantages [41,42].

2.4. Influence of Common Matrix Species

Figure S6 presented the effects of several common matrix species, including Cl^{-}, CO_3^{2-}, SO_4^{2-}, and humic acid, on the degradation efficiency of SMX in the SBCs/PI system. The concentrations of several common matrix species were selected according to previous literature [43]. As observed, the presence of Cl^{-}, SO_4^{2-}, and HA did not significantly inhibit the degradation of SMX in all SBCs/PI systems, and even a slight promotion effect was observed in SBC/500 and SBC/700 systems. Previous studies have shown that Cl^{-} may affect the degradation of organic pollutants in PI systems due to the reaction with reactive species such as $IO_3^{\bullet}$, while HA may also affect the degradation of organic pollutants due to the competition with reactive oxygen species [38,41]. This result suggested that the degradation of SMX by reactive oxygen species within the SBCs/PI system may not occupy a major role. Conversely, the presence of CO_3^{2-} produced a strong inhibition of SMX degradation for all SBCs/PI systems, which was most likely attributed to the pH effect of CO_3^{2-} addition to the solution (solution pH increased to 8.5 after the reaction). These results indicated that the SBCs/PI system has a strong resistance to the common matrix species in the water column.

2.5. Identification of Major Active Species and Possible Activation Mechanism

To identify the major active species and active sites for SMX degradation, a variety of chemical scavengers were employed, and their inhibitory extent against SMX degradation was compared. As depicted in Figure 6, when methanol and TBA [44,45] were used as quenchers for •OH radicals, the degradation efficiency of SMX was almost invariable for all SBCs/PI systems, indicating that the contribution of •OH radicals to the degradation of SMX was very slight in the system. Compared with the control group, the effect of furfuryl alcohol (FFA) addition on the degradation of SMX was not observable for all SBCs/PI systems, indicating the contribution of $^1O_2$ could be ignored [44,46]. In addition, to figure out the presence of $O_2^{\bullet-}$ in the SBCs/PI systems, chloroform was employed as a quencher for $O_2^{\bullet-}$ [47]. Similarly, the addition of chloroform showed no significant inhibition for the efficiency of SMX degradation in all SBCs/PI systems, while there was a slight inhibition for the rate of SMX degradation within all systems. The results revealed that $O_2^{\bullet-}$ did not play a dominant role in the SBCs/PI system. To exclude the role of higher valence metals in the activation of PI, excess dimethyl sulfoxide (DMSO) was introduced into the SBCs/PI system to observe its inhibitory effect on SMX degradation. The DMSO can be oxidized by high-valent iron oxide species to form dimethyl sulfone (DMSO2) through an oxygen atom transfer reaction [48,49]. As shown in Figure 6, the addition of 200 mM DMSO decreased the degradation efficiency of SMX by 5% and 1% in the SBC500/PI and SBC700/PI systems, respectively, and it produced an inhibitory effect on the SMX degradation rate in the SBCs/PI systems. In addition, the results of metal leaching experiments showed that the Fe-leaching concentration in all SBCs/PI systems was below the detection limit of atomic absorption spectroscopy (0.03 mg L^{-1}), indicating that the presence of high-valent Fe contributed minimally to the system.

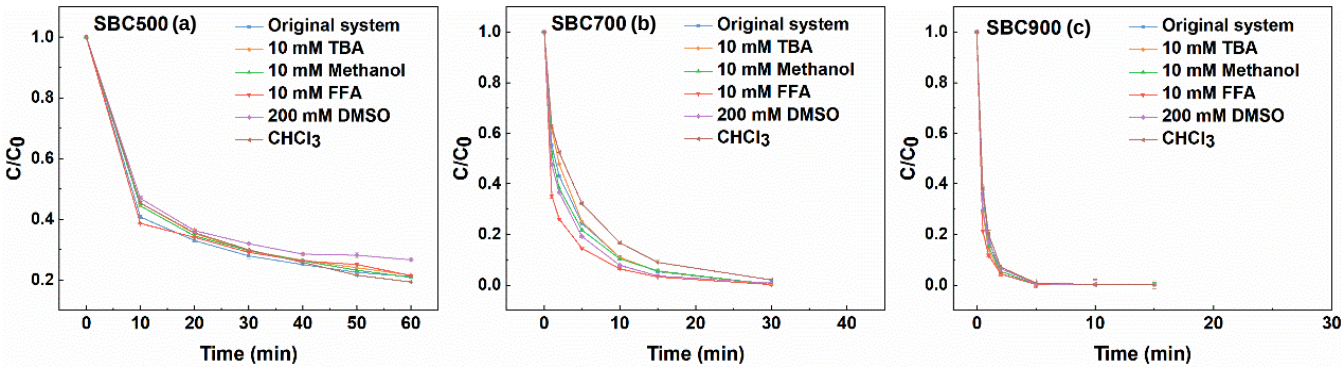

Figure 6. Influence of chemical scavengers on the degradation of SMX in various SBCs/PI systems.

EPR was employed to further characterize the active species in the SBCs/PI systems. As illustrated in Figure 7, 5,5-dimethyl-1-pyrrolidine-oxide DMPO (in water), DMPO (in methanol), and 2,2,6,6-tetramethylpiperidine (TEMP) were generally utilized to capture •OH radicals, $O_2^{\bullet-}$, and $^1O_2$. Compared to the H_2O+DMPO group, distinct characteristic signals of DMPO-•OH with an intensity ratio of 1:2:2:1 were observed in the DMPO+PI and DMPO+SBC/PI group, and the intensity of the peak in the SBC/PI system was slightly increased, which proved the presence of •OH in the PI alone and SBC/PI systems. Under acidic conditions, the oxygen-containing functional groups enriched in sludge-based biochar could react with them to produce •OH radicals [23]. DMPO was further utilized in methanol solution to identify the presence of $O_2^{\bullet-}$ in the system. Obvious signals of DMPO-$O_2^{\bullet-}$ (quadruple peaks of equal strength with hyperfine splitting) were detected in PI alone and SBC/PI systems compared with the blank group, which demonstrated the presence of $O_2^{\bullet-}$ in the SBC/PI system. This was confirmed in a previous study that IO_4^- could react with O_2 to form $O_2^{\bullet-}$ in the presence of dissolved oxygen [20]. In addition, no triple signals of 1:1:1 were found in any system when TEMP was used as a trapping agent for $^1O_2$, suggesting the absence of $^1O_2$ in the SBCs/PI systems. Simultaneously, to exclude the contribution of iodate radicals such as $IO_3^{\bullet}$ and $IO_4^{\bullet}$ in the system to the degradation of SMX, DMPO in the DMSO solution was employed to detect their presence [50]. However, no characteristic peaks of DMPO-$IO_3^{\bullet}$ or DMPO-$IO_4^{\bullet}$ were found, indicating that these iodate radicals were not present in the SBCs/PI systems. Thus, based on the above chemical quenching experiments and EPR analysis, various reactive oxygen species in the SBCs/PI system were excluded from contributing to SMX degradation, and the mechanism of SBCs activation of PI may involve an electron-mediated transfer mechanism.

To further confirm that the electron-mediated transfer mechanism was involved, electrochemical experiments were conducted. As shown in Figure 8a, the results of chronopotentiometry (i-t curve) showed that the current changed significantly when the periodate was added to the system at 100 s, indicating that a violent electron transfer process occurred between periodate and SBC, forming the SBC–PI complex. Similarly, a significant current change was also observed when SMX was added to the system at 250 s, demonstrating that electron transfer occurred between SMX and the PI-SBC complex through an electron-mediated transfer mechanism [51]. In addition, the EIS Nyquist plot of SBC500 in Figure 8b showed that SBC has good electron transfer process.

2.6. Toxicity Study in SBCs/PI Systems

The germination and average root length data of lettuce seeds are shown in Figure S7 and were employed to assess the solution toxicity after treatment with the SBCs/PI systems [52]. Apparently, after seven days of incubation, the presence of SMX and PI showed significant inhibition of lettuce growth compared to the deionized water control, indicating that both substances possess significant acute plant toxicity. In addition, the mix of PI and SMX showed a stronger inhibition of lettuce growth, which also indicates that the inactivated PI did not eliminate the effect of SMX toxicity. However, the SBCs exhibited a

notable elimination influence of both SMX and PI toxicity when added to the system. The toxicity effect decreased significantly with increasing pyrolysis temperature, indicating that the SBCs/PI system significantly attenuated the toxic effect of SMX.

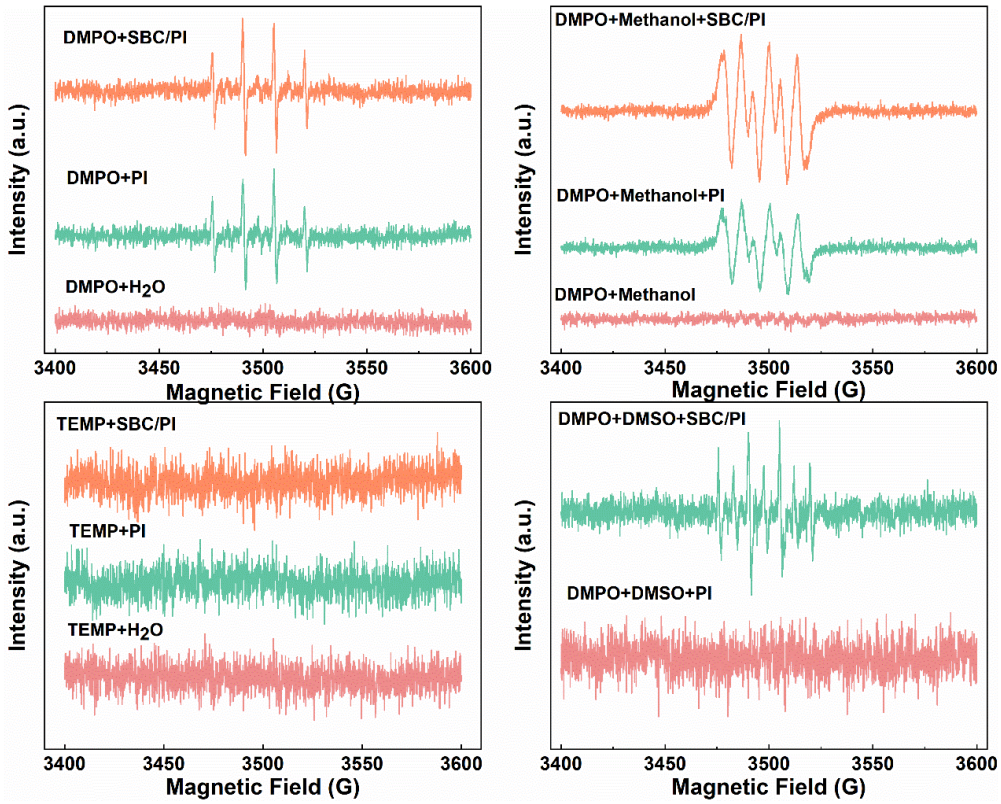

Figure 7. EPR spectrum on radicals in SBCs/PI systems captured by DMPO and TEMP.

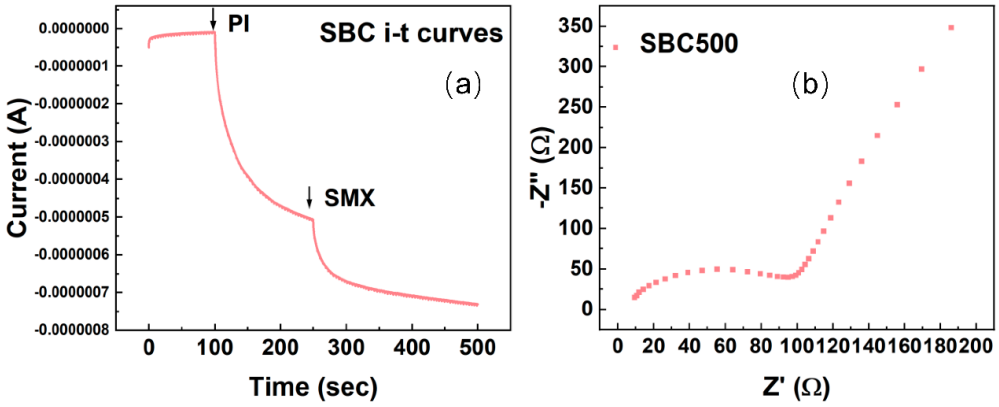

Figure 8. (**a**) The i-t curves of SBC500, (**b**) EIS Nyquist plot of SBC500.

3. Material and Methods

3.1. Materials

Hydrochloric acid (HCl) (36%), sodium hydroxide (NaOH) (≥96%), ethanol, sodium periodate ($NaIO_4$), humic acid, sodium chloride (NaCl) and sodium sulfate (Na_2SO_4) were provided by Sinopharm Chemical Reagent Co., Ltd. (Shanghai, China). Acetonitrile, tert-Butanol (TBA) methanol, and formic acid were provided by Shanghai Macklin Biochemical Co., Ltd (Shanghai, China). Sulfamethoxazole (98%), Furfuryl alcohol, 5,5-Dimethyl-1-pyrrolidine N-oxide (≥97%, DPMO), 2,2,6, 6-tetramethyl-4-piperidinol (≥97%, TEMP), and

dimethyl sulfoxide (DMSO) were provided by Shanghai Aladdin Biochemical Technology Co., Ltd (Shanghai, China).

The municipal dehydrated sewage sludge used in this study was obtained from the Tangxun Lake Municipal Wastewater Treatment Plant in Wuhan, China.

3.2. Preparation and Characterization of SBCs

The sludge biochar (SBCs) preparation was performed according to one of our previous studies [22]. The details of the characterization categories and electrochemical measurement methods can be found in Text S1.

3.3. Experimental Procedures and Analysis

The desorption experiments can be found in Text S2.

The typical experimental method for degradation and the detailed HPLC analysis parameters are presented in the supporting information (Text S3).

The acute ecotoxicity test was based on one of our previous studies [38] and is presented in Text S3.

4. Conclusions

The present study successfully prepared sludge biochar with four pyrolysis temperatures and investigated their ability to activate periodate to degrade SMX. The pore structure, the degree of graphitization, and the defect structure of sludge biochar become more superior as the pyrolysis temperature increases. The degradation of SMX by the SBCs/PI system was highly dependent on the initial pH of the solution and the dosage of SBCs. In addition, the presence of Cl^-, $SO_4{}^{2-}$, and HA did not inhibit the degradation of SMX in all SBCs/PI systems, while the presence of $CO_3{}^{2-}$ produced a strong inhibition of SMX degradation for all SBCs/PI systems. EPR and chemical quenching experiments excluded the effect of free-radical mechanism on the SBCs/PI system, and the degradation of SMX was further demonstrated by electrochemical experiments mainly through an electron-mediated transfer mechanism. The degradation of SMX by low-temperature pyrolysis of SBCs showed a definite radical contribution, while the degradation of SMX by high-temperature pyrolysis of SBCs was almost controlled by the electron transfer mechanism. Furthermore, acute toxicity measurements were completed by lettuce seed germination experiments, and the results showed that the SBCs/PI system showed better inhibition of SMX toxicity as the pyrolysis temperature increased.

Supplementary Materials: The following supporting information can be downloaded at: https://www.mdpi.com/article/10.3390/catal12111431/s1, Figure S1: The SEM images of SBCs; Figure S2: N2 adsorption and desorption curves of SBCs; Figure S3: The XPS spectra (N1s) of SBCs; Figure S4: The XPS spectra (C1s and O1s) of SBCs; Figure S5: The Zeta potential of SBCs; Figure S6: The background species on the degradation of SMX in the SBCs/PI system; Figure S7: The biotoxicity test of the SBCs/PI system; Table S1: The degradation rate of SMX at different systems; Table S2: Desorption experiment data of SBCs. Text S1. Characterization and electrochemical measurement methods; Text S2. The detailed procedures of the catalyst stability test experiments and desorption experiments; Text S3. Experimental procedures and analysis methods.

Author Contributions: Conceptualization, L.H. and L.Y.; methodology, S.Y.; software, D.K.; validation, S.Y. and Y.L.; formal analysis, L.W.; investigation, L.W.; resources, L.Y.; data curation, L.H., S.Y. and D.K.; writing—original draft preparation, L.H.; writing—review and editing, L.Y. and Z.Z.; visualization, L.H.; supervision, L.W.; project administration, Z.Z.; funding acquisition, L.Y. All authors have read and agreed to the published version of the manuscript.

Funding: This work was financially supported by the National Natural Science Foundation of China (No. 51878523, No. 52170171 and No. U1703120), the Fundamental Research Funds for the Central Universities (WUT: 193108003, 2019IVA032 and No. 215208002) and the Scottish Government's Rural and Environment Science and Analytical Service Division (RESAS).

Data Availability Statement: The data presented in this study are available on request from the corresponding author.

Acknowledgments: The authors acknowledge the financial support from the National Natural Science Foundation of China (No. 51878523, No. 52170171 and No. U1703120), the Fundamental Research Funds for the Central Universities (WUT: 193108003, 2019IVA032 and No. 215208002) and the Scottish Government's Rural and Environment Science and Analytical Service Division (RESAS).

Conflicts of Interest: The authors declare no conflict of interest.

References

1. Syed-Hassan, S.S.A.; Wang, Y.; Hu, S.; Su, S.; Xiang, J. Thermochemical processing of sewage sludge to energy and fuel: Fundamentals, challenges and considerations. *Renew. Sustain. Energy Rev.* **2017**, *80*, 888–913. [CrossRef]
2. Chen, Y.-D.; Wang, R.; Duan, X.; Wang, S.; Ren, N.-Q.; Ho, S.-H. Production, properties, and catalytic applications of sludge derived biochar for environmental remediation. *Water Res.* **2020**, *187*, 116390. [CrossRef] [PubMed]
3. Hu, M.; Gao, L.; Chen, Z.; Ma, C.; Zhou, Y.; Chen, J.; Ma, S.; Laghari, M.; Xiao, B.; Zhang, B.; et al. Syngas production by catalytic in-situ steam co-gasification of wet sewage sludge and pine sawdust. *Energy Convers. Manag.* **2016**, *111*, 409–416. [CrossRef]
4. Zhang, W.; Zheng, J.; Zheng, P.; Qiu, R. Atrazine immobilization on sludge derived biochar and the interactive influence of coexisting Pb(II) or Cr(VI) ions. *Chemosphere* **2015**, *134*, 438–445. [CrossRef]
5. Wu, Q.; Bao, X.; Guo, W.; Wang, B.; Li, Y.; Luo, H.; Wang, H.; Ren, N. Medium chain carboxylic acids production from waste biomass: Current advances and perspectives. *Biotechnol. Adv.* **2019**, *37*, 599–615. [CrossRef] [PubMed]
6. Fan, H.; Zhou, H.; Wang, J. Pyrolysis of municipal sewage sludges in a slowly heating and gas sweeping fixed-bed reactor. *Energy Convers. Manag.* **2014**, *88*, 1151–1158. [CrossRef]
7. Chen, Y.-d.; Ho, S.-H.; Nagarajan, D.; Ren, N.-q.; Chang, J.-S. Waste biorefineries—Integrating anaerobic digestion and microalgae cultivation for bioenergy production. *Curr. Opin. Biotechnol.* **2018**, *50*, 101–110. [CrossRef]
8. Samolada, M.C.; Zabaniotou, A.A. Comparative assessment of municipal sewage sludge incineration, gasification and pyrolysis for a sustainable sludge-to-energy management in Greece. *Waste Manag.* **2014**, *34*, 411–420. [CrossRef]
9. Wang, S.; Wang, J. Peroxymonosulfate activation by Co9S8@ S and N co-doped biochar for sulfamethoxazole degradation. *Chem. Eng. J.* **2020**, *385*, 123933. [CrossRef]
10. Liu, B.; Guo, W.; Wang, H.; Si, Q.; Zhao, Q.; Luo, H.; Ren, N. Activation of peroxymonosulfate by cobalt-impregnated biochar for atrazine degradation: The pivotal roles of persistent free radicals and ecotoxicity assessment. *J. Hazard. Mater.* **2020**, *398*, 122768. [CrossRef] [PubMed]
11. Jellali, S.; Khiari, B.; Usman, M.; Hamdi, H.; Charabi, Y.; Jeguirim, M. Sludge-derived biochars: A review on the influence of synthesis conditions on pollutants removal efficiency from wastewaters. *Renew. Sustain. Energy Rev.* **2021**, *144*, 111068. [CrossRef]
12. Wang, J.; Shen, M.; Gong, Q.; Wang, X.; Cai, J.; Wang, S.; Chen, Z. One-step preparation of ZVI-sludge derived biochar without external source of iron and its application on persulfate activation. *Sci. Total Environ.* **2020**, *714*, 136728. [CrossRef] [PubMed]
13. Ma, Y.; Yang, L.; Wu, L.; Li, P.; Qi, X.; He, L.; Cui, S.; Ding, Y.; Zhang, Z. Carbon nanotube supported sludge biochar as an efficient adsorbent for low concentrations of sulfamethoxazole removal. *Sci. Total Environ.* **2020**, *718*, 137299. [CrossRef] [PubMed]
14. Wang, S.; Wang, J. Activation of peroxymonosulfate by sludge-derived biochar for the degradation of triclosan in water and wastewater. *Chem. Eng. J.* **2019**, *356*, 350–358. [CrossRef]
15. Long, Y.; Dai, J.; Zhao, S.; Su, Y.; Wang, Z.; Zhang, Z. Atomically Dispersed Cobalt Sites on Graphene as Efficient Periodate Activators for Selective Organic Pollutant Degradation. *Environ. Sci. Technol.* **2021**, *55*, 5357–5370. [CrossRef]
16. Zhang, X.; Yu, X.; Yu, X.; Kamali, M.; Appels, L.; van der Bruggen, B.; Cabooter, D.; Dewil, R. Efficiency and mechanism of 2,4-dichlorophenol degradation by the UV/IO4− process. *Sci. Total Environ.* **2021**, *782*, 146781. [CrossRef]
17. Lee, Y.-C.; Chen, M.-J.; Huang, C.-P.; Kuo, J.; Lo, S.-L. Efficient sonochemical degradation of perfluorooctanoic acid using periodate. *Ultrason. Sonochem.* **2016**, *31*, 499–505. [CrossRef]
18. Chia, L.H.; Tang, X.M.; Weavers, L.K. Kinetics and mechanism of photoactivated periodate reaction with 4-chlorophenol in acidic solution. *Environ. Sci. Technol.* **2004**, *38*, 6875–6880. [CrossRef]
19. Du, J.; Tang, S.; Faheem; Ling, H.; Zheng, H.; Xiao, G.; Luo, L.; Bao, J.; Faheem; Ling, H. Insights into periodate oxidation of bisphenol A mediated by manganese. *Chem. Eng. J.* **2019**, *369*, 1034–1039. [CrossRef]
20. Bokare, A.D.; Choi, W. Singlet-Oxygen Generation in Alkaline Periodate Solution. *Environ. Sci. Technol.* **2015**, *49*, 14392–14400. [CrossRef]
21. Choi, Y.; Yoon, H.I.; Lee, C.; Vetrakova, L.; Heger, D.; Kim, K.; Kim, J. Activation of Periodate by Freezing for the Degradation of Aqueous Organic Pollutants. *Environ. Sci. Technol.* **2018**, *52*, 5378–5385. [CrossRef] [PubMed]
22. He, L.; Lv, L.; Pillai, S.C.; Wang, H.; Xue, J.; Ma, Y.; Liu, Y.; Chen, Y.; Wu, L.; Zhang, Z.; et al. Efficient degradation of diclofenac sodium by periodate activation using Fe/Cu bimetallic modified sewage sludge biochar/UV system. *Sci. Total Environ.* **2021**, *783*, 146974. [CrossRef] [PubMed]
23. He, L.; Shi, Y.; Chen, Y.; Shen, S.; Xue, J.; Ma, Y.; Zheng, L.; Wu, L.; Zhang, Z.; Yang, L. Iron-manganese oxide loaded sludge biochar as a novel periodate activator for thiacloprid efficient degradation over a wide pH range. *Sep. Purif. Technol.* **2022**, *288*, 120703. [CrossRef]

24. Tripathi, M.; Sahu, J.N.; Ganesan, P. Effect of process parameters on production of biochar from biomass waste through pyrolysis: A review. *Renew. Sustain. Energy Rev.* **2016**, *55*, 467–481. [CrossRef]
25. Zhao, L.; Cao, X.; Mašek, O.; Zimmerman, A. Heterogeneity of biochar properties as a function of feedstock sources and production temperatures. *J. Hazard. Mater.* **2013**, *256–257*, 1–9. [CrossRef]
26. Jin, J.; Li, Y.; Zhang, J.; Wu, S.; Cao, Y.; Liang, P.; Zhang, J.; Wong, M.H.; Wang, M.; Shan, S.; et al. Influence of pyrolysis temperature on properties and environmental safety of heavy metals in biochars derived from municipal sewage sludge. *J. Hazard. Mater.* **2016**, *320*, 417–426. [CrossRef]
27. Zhang, P.; Tan, X.; Liu, S.; Liu, Y.; Zeng, G.; Ye, S.; Yin, Z.; Hu, X.; Liu, N. Catalytic degradation of estrogen by persulfate activated with iron-doped graphitic biochar: Process variables effects and matrix effects. *Chem. Eng. J.* **2019**, *378*, 122141. [CrossRef]
28. Diao, Z.-H.; Dong, F.-X.; Yan, L.; Chen, Z.-L.; Qian, W.; Kong, L.-J.; Zhang, Z.-W.; Zhang, T.; Tao, X.-Q.; Du, J.-J.; et al. Synergistic oxidation of Bisphenol A in a heterogeneous ultrasound-enhanced sludge biochar catalyst/persulfate process: Reactivity and mechanism. *J. Hazard. Mater.* **2020**, *384*, 121385. [CrossRef]
29. Yan, J.; Han, L.; Gao, W.; Xue, S.; Chen, M. Biochar supported nanoscale zerovalent iron composite used as persulfate activator for removing trichloroethylene. *Bioresour. Technol.* **2015**, *175*, 269–274. [CrossRef]
30. Chen, H.; Wang, J. Degradation of sulfamethoxazole by ozonation combined with ionizing radiation. *J. Hazard. Mater.* **2021**, *407*, 124377. [CrossRef]
31. Bu, Q.; Wang, B.; Huang, J.; Deng, S.; Yu, G. Pharmaceuticals and personal care products in the aquatic environment in China: A review. *J. Hazard. Mater.* **2013**, *262*, 189–211. [CrossRef] [PubMed]
32. Choong, Z.-Y.; Gasim, M.F.; Lin, K.-Y.A.; Hamidon, T.S.; Hussin, H.; Oh, W.-D. Unravelling the formation mechanism and performance of nitrogen, sulfur codoped biochar as peroxymonosulfate activator for gatifloxacin removal. *Chem. Eng. J.* **2023**, *451*, 138958. [CrossRef]
33. Yang, Z.; Hou, J.; Wu, J.; Miao, L. The effect of carbonization temperature on the capacity and mechanisms of Pb(II) adsorption by microalgae residue-derived biochar. *Ecotoxicol. Environ. Saf.* **2021**, *225*, 112750. [CrossRef] [PubMed]
34. Ren, N.; Tang, Y.; Li, M. Mineral additive enhanced carbon retention and stabilization in sewage sludge-derived biochar. *Process Saf. Environ. Prot.* **2018**, *115*, 70–78. [CrossRef]
35. Ho, S.-H.; Chen, Y.-D.; Yang, Z.-K.; Nagarajan, D.; Chang, J.-S.; Ren, N.-Q. High-efficiency removal of lead from wastewater by biochar derived from anaerobic digestion sludge. *Bioresour. Technol.* **2017**, *246*, 142–149. [CrossRef] [PubMed]
36. Chen, X.; Oh, W.-D.; Hu, Z.-T.; Sun, Y.-M.; Webster, R.D.; Li, S.-Z.; Lim, T.-T. Enhancing sulfacetamide degradation by peroxymonosulfate activation with N-doped graphene produced through delicately-controlled nitrogen functionalization via tweaking thermal annealing processes. *Appl. Catal. B Environ.* **2018**, *225*, 243–257. [CrossRef]
37. Liu, S.; Lai, C.; Zhou, X.; Zhang, C.; Chen, L.; Yan, H.; Qin, L.; Huang, D.; Ye, H.; Chen, W.; et al. Peroxydisulfate activation by sulfur-doped ordered mesoporous carbon: Insight into the intrinsic relationship between defects and 1O2 generation. *Water Res.* **2022**, *221*, 118797. [CrossRef]
38. He, L.; Yang, S.; Shen, S.; Ma, Y.; Chen, Y.; Xue, J.; Wang, J.; Zheng, L.; Wu, L.; Zhang, Z.; et al. Novel insights into the mechanism of periodate activation by heterogeneous ultrasonic-enhanced sludge biochar: Relevance for efficient degradation of levofloxacin. *J. Hazard. Mater.* **2022**, *434*, 128860. [CrossRef]
39. Ji, Y.; Fan, Y.; Liu, K.; Kong, D.; Lu, J. Thermo activated persulfate oxidation of antibiotic sulfamethoxazole and structurally related compounds. *Water Res.* **2015**, *87*, 1–9. [CrossRef]
40. Fan, S.; Wang, Y.; Wang, Z.; Tang, J.; Tang, J.; Li, X. Removal of methylene blue from aqueous solution by sewage sludge-derived biochar: Adsorption kinetics, equilibrium, thermodynamics and mechanism. *J. Environ. Chem. Eng.* **2017**, *5*, 601–611. [CrossRef]
41. Li, X.; Liu, X.; Qi, C.; Lin, C. Activation of periodate by granular activated carbon for acid orange 7 decolorization. *J. Taiwan Inst. Chem. Eng.* **2016**, *68*, 211–217. [CrossRef]
42. Li, X.; Liu, X.; Lin, C.; Qi, C.; Zhang, H.; Ma, J. Enhanced activation of periodate by iodine-doped granular activated carbon for organic contaminant degradation. *Chemosphere* **2017**, *181*, 609–618. [CrossRef] [PubMed]
43. Oh, W.-D.; Lua, S.-K.; Dong, Z.; Lim, T.-T. Performance of magnetic activated carbon composite as peroxymonosulfate activator and regenerable adsorbent via sulfate radical-mediated oxidation processes. *J. Hazard. Mater.* **2015**, *284*, 1–9. [CrossRef]
44. Pan, X.; Chen, J.; Wu, N.; Qi, Y.; Xu, X.; Ge, J.; Wang, X.; Li, C.; Qu, R.; Sharma, V.K.; et al. Degradation of aqueous 2,4,4′-Trihydroxybenzophenone by persulfate activated with nitrogen doped carbonaceous materials and the formation of dimer products. *Water Res.* **2018**, *143*, 176–187. [CrossRef] [PubMed]
45. Yao, J.; Yu, Y.; Qu, R.; Chen, J.; Huo, Z.; Zhu, F.; Wang, Z. Fe-Activated Peroxymonosulfate Enhances the Degradation of Dibutyl Phthalate on Ground Quartz Sand. *Environ. Sci. Technol.* **2020**, *54*, 9052–9061. [CrossRef] [PubMed]
46. Sun, H.; He, F.; Choi, W. Production of Reactive Oxygen Species by the Reaction of Periodate and Hydroxylamine for Rapid Removal of Organic Pollutants and Waterborne Bacteria. *Environ. Sci. Technol.* **2020**, *54*, 6427–6437. [CrossRef]
47. Zhu, H.; Guo, A.; Wang, S.; Long, Y.; Fan, G.; Yu, X. Efficient tetracycline degradation via peroxymonosulfate activation by magnetic Co/N co-doped biochar: Emphasizing the important role of biochar graphitization. *Chem. Eng. J.* **2022**, *450*, 138428. [CrossRef]
48. Peng, L.; Duan, X.; Shang, Y.; Gao, B.; Xu, X. Engineered carbon supported single iron atom sites and iron clusters from Fe-rich Enteromorpha for Fenton-like reactions via nonradical pathways. *Appl. Catal. B Environ.* **2021**, *287*, 119963. [CrossRef]

49. Li, Y.; Yang, T.; Qiu, S.; Lin, W.; Yan, J.; Fan, S.; Zhou, Q. Uniform N-coordinated single-atomic iron sites dispersed in porous carbon framework to activate PMS for efficient BPA degradation via high-valent iron-oxo species. *Chem. Eng. J.* **2020**, *389*, 124382. [CrossRef]
50. Chen, L.; Duan, J.; Du, P.; Sun, W.; Lai, B.; Liu, W. Accurate identification of radicals by in-situ electron paramagnetic resonance in ultraviolet-based homogenous advanced oxidation processes. *Water Res.* **2022**, *221*, 118747. [CrossRef]
51. Dong, X.; Ren, B.; Zhang, X.; Liu, X.; Sun, Z.; Li, C.; Tan, Y.; Yang, S.; Zheng, S.; Dionysiou, D.D. Diatomite supported hierarchical 2D CoNi3O4 nanoribbons as highly efficient peroxymonosulfate catalyst for atrazine degradation. *Appl. Catal. B Environ.* **2020**, *272*, 118971. [CrossRef]
52. Wang, J.; Shen, M.; Wang, H.; Du, Y.; Zhou, X.; Liao, Z.; Wang, H.; Chen, Z. Red mud modified sludge biochar for the activation of peroxymonosulfate: Singlet oxygen dominated mechanism and toxicity prediction. *Sci. Total Environ.* **2020**, *740*, 140388. [CrossRef] [PubMed]